Analysis of subband structures and optical properties of periodic strained quantum wires by a finite element method

Ishigaki, T.
Ogawa, Matsuto
Morita M.
Miyoshi, Tanroku

(Citation)
Journal of Applied Physics,91(9):5815-5819

(Issue Date)
2002-05-01

(Resource Type)
journal article

(Version)
Version of Record

(URL)
https://hdl.handle.net/20.500.14094/90000825

Analysis of subband structures and optical properties of periodic strained quantum wires by a finite element method

T. Ishigaki, M. Ogawa,[a] M. Morita, and T. Miyoshi
Department of Electrical and Electronics Engineering, Kobe University, 1 Rokkodai, Nada, Kobe 657-8501, Japan

(Received 6 August 2001; accepted for publication 21 January 2002)

We present theoretical investigations of subband structures and optical absorption properties of periodic quantum wires. The calculation is based on the multiband effective mass theory, where effects such as the valence-band mixing effects, the dependence of crystallographic orientation, and the strain effect using a total energy minimization technique are duly taken into account. We use the finite element method to solve the eigenvalue problem with periodic boundary conditions for the quasitwo-dimensional quantum confinement effect. We study strain effects on subband structures and optical properties, and dependence of the optical properties on the crystallographic orientation.
 [DOI: 10.1063/1.1459098]

I. INTRODUCTION

Semiconductor quantum wire (QWR) lasers with low threshold current, wider bandwidth, and narrower spectral linewidth have become essential as light sources for optical communication systems. They are promising for possible polarization-stabilized vertical cavity surface-emitting lasers (VCSELs). So far, various kinds of QWRs with various cross sections and various crystallographic orientations[1–4] have been studied to fabricate uniformly high density QWRs and achieve successful application to QWR lasers.

In the valence band of such QWRs, a reduction of the dimensionality enhances heavy hole (HH) and light hole (LH) mixing and increases the nonparabolicities compared with those of quantum wells. So far, almost all the QWRs fabricated, such as T-shaped, V-grooved, corrugated QWRs, have been classified as quasibounded quantum wires which are weakly bounded in the lateral direction and their properties have not yet been fully understood. On the other hand, the strain effect which is inherent and is caused by lattice mismatch between the QWR and barrier material strongly depends on the cross-sectional shape of the QWR. Therefore, we have to know the exact strain tensor distribution in QWRs for optimal design of the lasers, since strain significantly affects the subband structures. In addition, the crystal orientation of QWRs is also an effective parameter by which to optimize laser performance. Therefore, it is quite important to analyze the subband structures and the optical properties of strained and arbitrarily ($[hkl]$-) oriented QWRs precisely for optimal design of QWR based optical devices.

In this article, we present an analysis of the strain effect on the subband structures and optical properties of $[hkl]$-oriented quasibounded QWRs (periodic in the lateral direction). Our calculation uses a finite element method (FEM) based on multiband-effective-mass theory[5] in which the effects of the valence-band mixing, strain, spinor transform associated with the coordinate transform, and lateral periodic boundary condition are taken into account.

In Sec. II, we briefly describe the calculation procedure based on the multiband $\mathbf{k}\times\mathbf{p}$ perturbation method including the strain effect. The effect of the crystal orientation[6,7] on both the strain tensor distribution and the subband structures is described by considering not only a coordinate transform but also a spinor transform. In Sec. III, we apply our model to an analysis of the strain tensor distribution, subband structures, and optical properties of corrugated QWRs with emphasis on the importance of the strain effect and the crystallographic orientation. Finally we summarize our conclusions.

II. CALCULATION PROCEDURE

A. Band calculation

First, we consider a strained QWR oriented in the [010] direction which we take as the y axis. For calculation of the optical properties, it is necessary to know both the subband structures (E-k_y dispersion relations) and the wave functions of carriers in the QWR. For simplicity, we assume that the conduction and valence bands are decoupled, and the parabolic band approximation with an effective mass m_c^* is applied to the conduction band. This can be justified by the fact that the band gap energy ($\geqslant$1 eV) is larger than differences in the subband energy. When we calculate the subband structures of the valence band of the QWR, we use the 4×4 Pikus–Bir Hamiltonian[8] including the strain effect:

$$\boldsymbol{H}(k_x,k_y,k_z)=\begin{array}{c}\begin{matrix}\quad|1{:}\mathrm{HH}\uparrow\rangle & |2{:}\mathrm{LH}\uparrow\rangle & |3{:}\mathrm{LH}\downarrow\rangle & |4{:}\mathrm{HH}\downarrow\rangle\end{matrix}\\ \begin{pmatrix} P+Q & -S & R & 0 \\ -S^{\dagger} & P-Q & 0 & R \\ R^{\dagger} & 0 & P-Q & S \\ 0 & R^{\dagger} & S^{\dagger} & P+Q \end{pmatrix}\end{array} \tag{2.1}$$

All matrix elements are written in terms of Lüttinger parameters, γ_1, γ_2, γ_3, deformation potentials, a_v, b, d, and strain tensors ε_{ij} $(i,j=x,y,z)$.

[a]Author to whom correspondence should be addressed; electronic mail: ogawa@eedept.kobe-u.ac.jp

The basis function set u_j^v for the matrix operator in Eq. (2.1) comprises the Bloch functions at the top of valence band, which are expressed as

$$\left|\frac{3}{2},\frac{3}{2}\right\rangle = u_{1,0}^v = -\frac{1}{\sqrt{2}}|(X+iY)\uparrow\rangle,$$

$$\left|\frac{3}{2},\frac{1}{2}\right\rangle = u_{2,0}^v = -\frac{1}{\sqrt{6}}|(X+iY)\downarrow -2Z\uparrow\rangle,$$

$$\left|\frac{3}{2},-\frac{1}{2}\right\rangle = u_{3,0}^v = \frac{1}{\sqrt{6}}|(X-iY)\uparrow +2Z\downarrow\rangle,$$

$$\left|\frac{3}{2},-\frac{3}{2}\right\rangle = u_{4,0}^v = \frac{1}{\sqrt{2}}|(X-iY)\downarrow\rangle. \tag{2.2}$$

When we analyze the valence-subband structure of an $[hkl]$-oriented strained QWR, we transform the original crystal coordinate system (x,y,z) into another one (x',y',z') to match the crystallographic orientation. In addition, the wave vectors are also transformed to

$$\begin{pmatrix} k_x \\ k_y \\ k_z \end{pmatrix} = \boldsymbol{R}^t(\phi,\theta,\delta)\begin{pmatrix} k_{x'} \\ k_{y'} \\ k_{z'} \end{pmatrix}, \tag{2.3}$$

where the coordinate rotation matrix is defined by, respectively,

$$\boldsymbol{R}(\phi,\theta,\delta) = \begin{pmatrix} \cos\delta\cos\theta\cos\phi+\sin\delta(-\sin\phi) & \cos\delta\cos\theta\sin\phi+\sin\delta\cos\phi & \cos\delta(-\sin\phi) \\ -\sin\delta\cos\theta\cos\phi+\cos\delta(-\sin\phi) & -\sin\delta\cos\theta\sin\phi+\cos\delta\cos\phi & -\sin\delta(-\sin\theta) \\ \sin\theta\cos\phi & \sin\theta\sin\phi & \cos\theta \end{pmatrix} \tag{2.4}$$

Using Eq. (2.3), we replace k_x, k_y, and k_z by $k_{x'}$, $k_{y'}$, and $k_{z'}$, respectively, in Eq. (2.1). Then the Hamiltonian should be transformed taking into account the spinor transform[6]

$$\boldsymbol{H}^v = \boldsymbol{R}_z^v(\delta)\boldsymbol{R}_y^v(\theta)\boldsymbol{R}_z^v(\phi)\boldsymbol{H}^v\boldsymbol{R}_z^v(\phi)^\dagger\boldsymbol{R}_y^v(\theta)^\dagger\boldsymbol{R}_z^v(\theta)^\dagger, \tag{2.5}$$

where the spinor rotation matrices are defined by

$$\boldsymbol{R}_z^v(\phi) = \begin{pmatrix} \exp(i\frac{3}{2}\phi) & 0 & 0 & 0 \\ 0 & \exp(i\frac{1}{2}\phi) & 0 & 0 \\ 0 & 0 & \exp(-i\frac{1}{2}\phi) & 0 \\ 0 & 0 & 0 & \exp(-i\frac{3}{2}\phi) \end{pmatrix}, \tag{2.6}$$

and

$$\boldsymbol{R}_y^v(\theta) = \begin{pmatrix} a^3 & \sqrt{3}a^2b & \sqrt{3}ab^2 & b^3 \\ -\sqrt{3}a^2b & a^3-2ab^2 & -b^3+2a^2b & \sqrt{3}ab^2 \\ \sqrt{3}ab^2 & b^3-2a^2b & a^3-2ab^2 & \sqrt{3}a^2b \\ -b^3 & \sqrt{3}ab^2 & -\sqrt{3}a^2b & a^3, \end{pmatrix},$$

$$[a=\cos(\theta/2), b=\sin(\theta/2)]. \tag{2.7}$$

At this time, the base function set is transformed to

$$\begin{pmatrix} u_{1,0}^{v\prime} \\ u_{2,0}^{v\prime} \\ u_{3,0}^{v\prime} \\ u_{4,0}^{v\prime} \end{pmatrix} = [\boldsymbol{R}_z^v(\delta)\boldsymbol{R}_y^v(\theta)\boldsymbol{R}_z^v(\phi)]^* \begin{pmatrix} u_{1,0}^v \\ u_{2,0}^v \\ u_{3,0}^v \\ u_{4,0}^v \end{pmatrix}. \tag{2.8}$$

In the QWR, the wave numbers k_x and k_z are substituted by operators as $k_x \rightarrow i\partial/\partial x$ and $k_z \rightarrow -i\partial/\partial z$, respectively, since the system is quantized in both the x and z directions.

Finally, we obtain the eigenvalue equation, $\boldsymbol{H}^{v\prime}(k_y)\Phi_{k_y}^v(x,z) = E(k_y)\Phi_{k_y}^v(x,z)$, which contains the effects of strain and crystallographic orientation. We can numerically solve this eigenvalue equation using a FEM based on the Galerkin method presented in the literature.[9]

B. Strain calculation

To calculate the band structures of the strained QWR using the Pikus–Bir Hamiltonian, Eq. (2.1), we have to know the strain tensor distribution. In the QWR, we cannot, apply the biaxial strain adopted in conventional analysis of quantum wells (QWs), so we use the energy theorem and assume the plain strain problem:

$$\varepsilon_{yy} = 0. \tag{2.9}$$

At this time, the Hooke's law is expressed as

$$\begin{bmatrix} \sigma_{xx} \\ \sigma_{zz} \\ \sigma_{zx} \end{bmatrix} = \begin{bmatrix} C_{11} & C_{12} & 0 \\ C_{12} & C_{11} & 0 \\ 0 & 0 & C_{44} \end{bmatrix} \left[\begin{bmatrix} \varepsilon_{xx} \\ \varepsilon_{zz} \\ \varepsilon_{zx} \end{bmatrix} - \begin{bmatrix} \varepsilon_{xx0} \\ \varepsilon_{zz0} \\ \varepsilon_{zx0} \end{bmatrix} \right], \tag{2.10}$$

where ε_{ij0} are initial strain tensors. In this article, we consider strained-layer quantum wires, assuming that the growth

direction is along the z axis, since stress for z direction is free, which means the stress tensor for the z axis σ_{zz} is zero. Then the initial strain tensor becomes

$$\begin{bmatrix} \sigma_{xx} \\ 0 \\ 0 \end{bmatrix} = \begin{bmatrix} C_{11} & C_{12} & 0 \\ C_{12} & C_{11} & 0 \\ 0 & 0 & C_{44} \end{bmatrix} \begin{bmatrix} \dfrac{a_0-a}{a} \\ \varepsilon_{zz0} \\ 0 \end{bmatrix}, \tag{2.11}$$

$$\varepsilon_0 = \frac{a_0-a}{a}\theta(\boldsymbol{r}) \begin{bmatrix} 1 \\ -\dfrac{C_{12}}{C_{11}} \\ 0 \end{bmatrix} \quad (\theta)(\boldsymbol{r}) = \begin{cases} 1 & \text{wire} \\ 0 & \text{barrier.} \end{cases}$$

Analysis of the system begins by adopting a coordinate system (x',y',z') which is related to the coordinate system (x,y,z) of the primary crystallographic axes of the substrate by the rotation $\boldsymbol{U}$[7]

$$\boldsymbol{U} = \boldsymbol{R}^t. \tag{2.12}$$

The relationship between coordinate systems for vectors and tensors is expressed as

$$\begin{cases} d'_\alpha = U_{\beta\alpha} d_\beta, \\ \varepsilon'_{\alpha\beta} = U_{i\alpha} U_{j\beta} \varepsilon_{ij}, \\ C'_{\gamma\delta kl} = U_{\alpha\gamma} U_{\beta\delta} U_{ik} U_{jl} C_{\alpha\beta ij} \end{cases}$$

$$(\alpha,\beta,\gamma,\delta,i,j,k,l = x,y,z),$$

where summation convention is used over indices that are repeated.

C. Optical properties

Once we have obtained both the band structures and the wave functions of the QWR, the optical absorb coefficient α in the QWR is given by

$$\alpha(\omega) = \frac{\omega \mu_0 c_0}{\pi n_r S} \int_0^\infty |\boldsymbol{e}\cdot\boldsymbol{M}_{vn}^{cm}(k_y)|^2 \times \frac{\hbar/\tau_{\text{in}}}{[E_{cv}(k_y) - \hbar\omega]^2 + (\hbar/\tau_{\text{in}})^2} dk_y, \tag{2.13}$$

where S is the QWR's area, $\boldsymbol{e}$ is the polarization vector, n and m are the indices of the conduction subband and valence subband, respectively, n_r is the refractive index, μ_0 is the permeability of vacuum, c_0 is the light speed, $\hbar$ is the Planck constant divided by 2π, and τ_{in} is the relaxation time in the band. The momentum matrix elements $\boldsymbol{M}$ are

$$|\boldsymbol{e}\cdot\boldsymbol{M}(k_y)_{vn}^{cm\uparrow}|^2 = |\boldsymbol{e}\cdot\boldsymbol{M}(k_y)_{vn}^{cm\uparrow}|^2 + |\boldsymbol{e}\cdot\boldsymbol{M}(k_y)_{vn}^{cm\downarrow}|^2, \tag{2.14}$$

$$|\boldsymbol{e}\cdot\boldsymbol{M}(k_y)_{vn}^{cm\uparrow}|^2 = |\langle \Phi_m^{c\uparrow} | \boldsymbol{e}\cdot\boldsymbol{e}\boldsymbol{r} | \Phi_n^v \rangle|^2$$

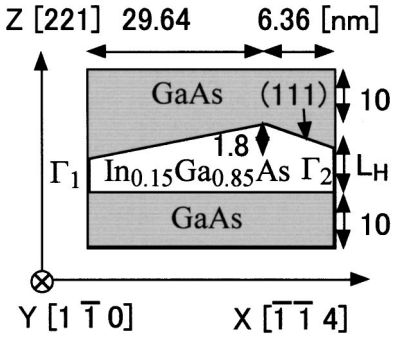

FIG. 1. Schematic structure of the [221] oriented $In_{0.15}Ga_{0.85}As$ corrugated quantum wire under investigation. Periodic boundary conditions are applied to the left and right sides (Γ_1 and Γ_2).

$$= \left| \sum_{j=1}^{4} \langle G_{m,1}^{c\uparrow} u_{1,0}^c | \boldsymbol{e}\cdot\boldsymbol{e}\boldsymbol{r} | G_{n,j}^v u_{j,0}^v \rangle \right|^2 \tag{2.15}$$

$$= \left| \sum_{j=1}^{4} \langle G_{m,1}^{c\uparrow} | G_{n,j}^v \rangle \langle iS\uparrow | \boldsymbol{e}\cdot\boldsymbol{e}\boldsymbol{r} | u_{j,0}^v \rangle \right|^2,$$

where G^c and G^v are the conduction and valence envelope functions, respectively. In the rotated coordinate system (x',y',z'), we have to use Eq. (2.8) as the base functions.

III. NUMERICAL RESULTS

Based on the calculation procedure presented in Sec. II, we have confined ourselves to analysis of the subband structures and wave functions of the corrugated GaAs/$In_{0.15}Ga_{0.85}As$/GaAs QWR shown in Fig. 1. This structure has the same structure as that fabricated in the Hiyamizu Laboratory at Osaka University. It was grown on a (221)-oriented GaAs substrate by molecular-beam epitaxy (MBE), and the InGaAs layer became corrugated with high uniformity as reported in the literature.[10]

TABLE I. Parameters used in calculation of the QWRs.

Parameter	GaAs	InAs
α_0 (Å)	5.6532	6.0584
E_g (eV)	1.519	0.42
ΔE_c (eV)	0.0852	
ΔE_v (eV)	0.1278	
γ_1	6.85	20.4
γ_2	2.10	8.3
γ_3	2.90	9.1
m_c^*/m_0	0.067	0.023
a_c (eV)	−7.17	−5.08
a_v (eV)	1.16	1.00
$a = a_c - a_v$ (eV)	−8.33	−6.08
b (eV)	−1.7	−1.8
d (eV)	−4.55	−3.6
C_{11} ($\times 10^{11}$ dyne/cm^2)	11.879	8.329
C_{12} ($\times 10^{11}$ dyne/cm^2)	5.376	4.526
C_{44} ($\times 10^{11}$ dyne/cm^2)	5.94	3.96
n_r	4.025	4.558

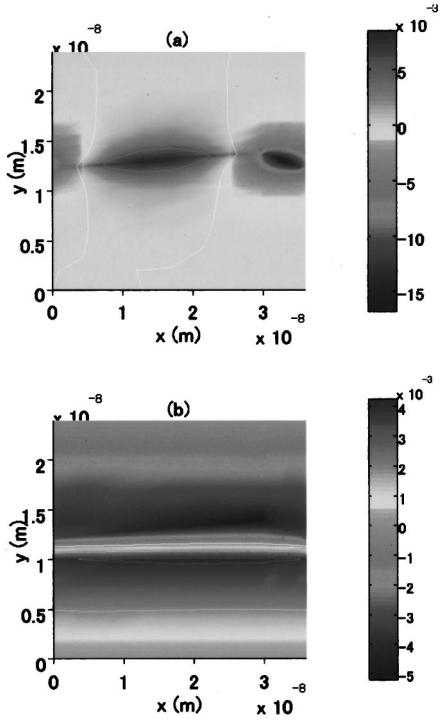

FIG. 2. Distributions of (a) x and (b) z displacements using the energy theorem on strain.

In our calculation, the energy gap and effective mass of $In_xGa_{1-x}As$ is calculated using the relations

$$E_g(\Gamma)=0.422+0.7x+0.4x^2(\mathrm{eV}),$$
$$m_e^*/m_0=0.025(1-x)+0.071x-0.0163x(1-x). \tag{3.1}$$

The other material parameters were determined by linearly interpolating the values of InAs and GaAs (Vegard's rule),

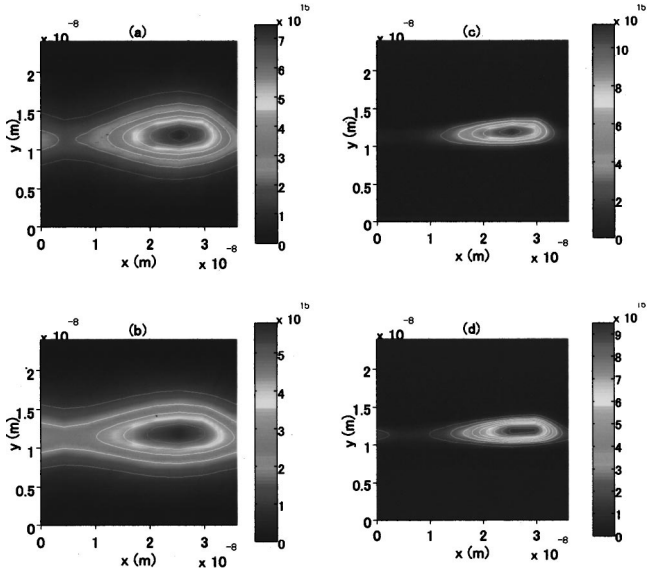

FIG. 3. Comparison of the envelope wave function of the first conduction subband at the Γ point (a) with the strain effect and (b) without the strain effect. The heavy hole (HH) components (G_1 and G_4) of the envelope wave function of the first valence subband at the Γ point (c) with the strain effect and (d) without the strain effect.

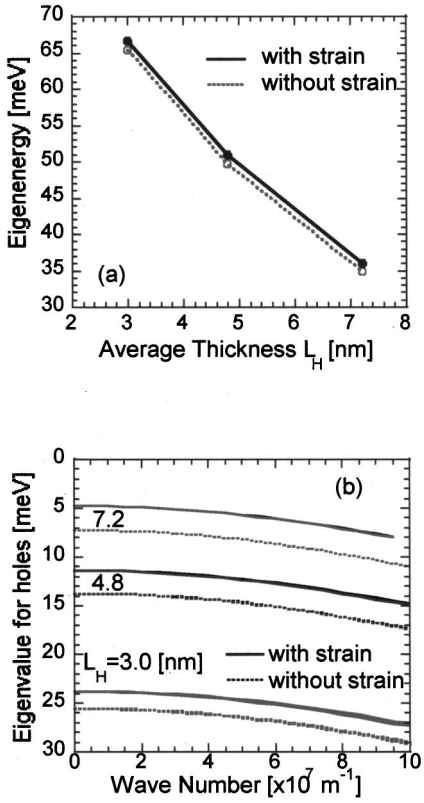

FIG. 4. (a) Shifts in energy of the first conduction subband (at $k_y=0$) from the strain effect. (b) Shifts of the first and second valence subbands ($E-k_y$ dispersion relations). The origin of the energies are set, respectively, at the conduction band bottom and valence band top of InGaAs.

given in Table I.[8] To solve the generalized eigenvalue problem, we use the Lanczos tridiagonalization procedure with sparse matrix format.[11]

Figures 2(a) and 2(b) show the calculated strain displacement distributions. Because of the boundary condition, under which the displacements are set to zero on the top and bottom boundaries, the displacements in the z direction are 10 times smaller in magnitude (10^{-3}) than those in the x direction (10^{-2}). On the other hand, because the lateral (x) displacements are concentrated on the GaAs/InGaAs upper boundary, the roof of the QWR is compressed from both sides. This is due to initial compressive strain in the structure. It should be noted that these results of the QWR are quite different from those of a usual strained QW.[12]

We also show the wave functions at the Γ point ($k_y=0$) both with strain and without strain effects in Figs. 3(a)–3(d), respectively. Due to the two-dimensional strain effects, that the confinement potential for carriers from the strain tensors becomes enhanced around the roof of the QWR, the wave functions are stressed out of the roof region and become similar to those of a quantum well.

Figures 4(a) and 4(b) show the energy shifts of the subband structures from strain effects. The shifts in energy of both the conduction subband and valence subband are small, and the valence-subband $E-k_y$ dispersions are almost parabolic. At the Γ point ($k_y=0$ and the Bloch periodic wave number in the x direction, $K_x=0$), the first and second subbands are degenerate, and the occupied LH percentage is only 1%. This is because the shape of the confinement po-

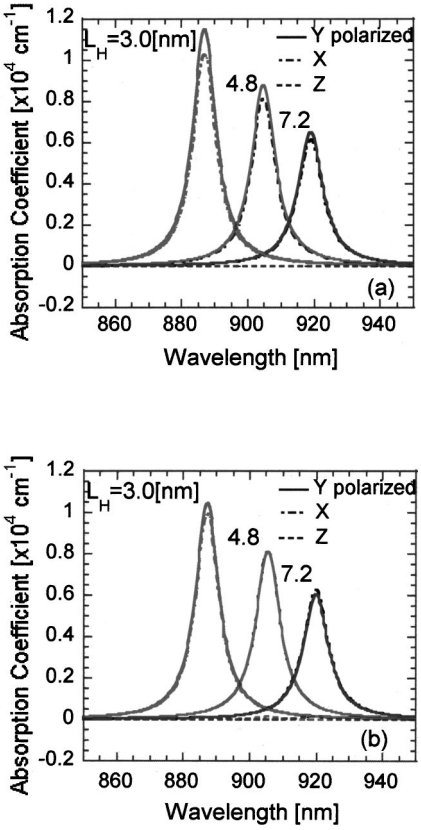

FIG. 5. Optical absorption coefficients (a) with the strain effect and (b) without the strain effect.

tential is QW like, and two-dimensional quantum confinement effects in the x direction are weak.

From these subband structures, we have calculated the optical absorption coefficients in Figs. 5(a) and 5(b), where integration over wave number k_y in Eq. (2.13) is only around the band edge ($k_y \sim 5.0\times 10^7$ m^{-1} at a Bloch wave number of $K_x=0$), which is sufficiently large to show the optical properties of the QWR. The difference between x- and y-polarized coefficients increases with the layer height getting thinner (layer height $=7.2\rightarrow 3.0$ nm), and the z-polarized coefficient is almost zero in the quantum wells. In comparing the experimental results,[10] one sees there is a difference between the wavelength and x-and y-polarized coefficients when the layer thickness becomes thinner. This is, we believe, due to uncertainty in the conduction band offset ΔE_c in the GaAs/InGaAs system and the size of the fluctuation of the QWRs fabricated.

We show the dependence of the degree of optical polarization which is calculated by Eq. (3.2) on the crystallographic orientation in Fig. 6.

$$P=(I_y-I_x)/(I_y+I_x), \tag{3.2}$$

where I_x and I_y are calculated by integrating the x-and y-polarized absorption coefficients, respectively. The degree of polarization P increases as the z-axis orientation becomes inclined from (001) towards (110) with an increase in the band mixing effect. Since the polarization stability of a laser diode is important for optical communication applications,

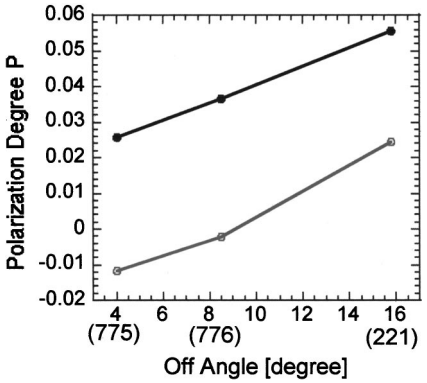

FIG. 6. Dependence of the degree of optical polarization on the crystallographic orientation.

this result may be helpful in optimizing laser characteristics of lasers fabricated on oriented substrates.

IV. CONCLUSIONS

Based on the multiband-effective-mass theory, we have formulated a subband calculation procedure for periodic strained QWRs. We have taken into account the effects of the band mixing between HH and LH states, periodic boundary conditions, strain effects, and the crystallographic orientation. The absorption coefficient of QWRs can be calculated from the results of our procedure.

We have applied our calculation to an analysis of the properties of a corrugated InGaAs/GaAs QWR. It was found that the periodic shapes of the confinement potential and the strain effects significantly affect the optical absorption properties. Furthermore, it was also found that the orientation of QWRs changes the degree of polarization. These results show that our method of band structure design can be used to improve laser characteristics.

ACKNOWLEDGMENTS

The authors would like to thank members of the Hiyamizu Laboratory, specifically Professor S. Hiyamizu, S. Shimomura, Dr. Higashiwaki, and Ohno, for their experimental data and for useful comments on the subject of this article.

[1] L. Pfeiffer, Appl. Phys. Lett. **56**, 1697 (1990).
[2] Y. Nagamune, Y. Arakawa, S. Tsukamoto, M. Nishioka, S. Sasaki, and N. Miura, Phys. Rev. Lett. **69**, 2963 (1992).
[3] M. Higashiwaki, M. Yamamoto, T. Higuchi, S. Shimomura, A. Adachi, Y. Okamoto, N. Sano, and S. Hiyamizu, Jpn. J. Appl. Phys., Part 1 **35**, 606 (1996).
[4] K. Inoue, K. Kimura, K. Maehashi, S. Hasegawa, H. Nakashima, M. Iwane, O. Matsuda, and K. Murase, J. Cryst. Growth **127**, 1041 (1993).
[5] J. J. Lüttinger and W. Kohn, Phys. Rev. **97**, 869 (1955).
[6] R. P. Feynman, *The Feynman Lectures on Physics III* (Addison–Wesley, Reading, MA, 1965), Chap. 6.
[7] J. M. Hinckley and J. Singh, Phys. Rev. B **42**, 3546 (1990).
[8] S. L. Chuang, *Physics of Optoelectronic Devices* (Wiley, New York, 1995).
[9] M. Ogawa, T. Kunimasa, T. Ito, and T. Miyoshi, J. Appl. Phys. **84**, 3242 (1998).
[10] Y. Ohno, Master's thesis, Osaka University, Osaka, Japan 2000.
[11] C. Lanczos, J. Res. Natl. Bur. Stand. **45**, 255 (1950).
[12] E. Yablonovitch, J. Lightwave Technol. **6**, 1292 (1988).